2003

The Temporally Filtered Navier-Stokes Equations: Propertes of the Residual Stress

C. D. Pruett

T. B. Gatski

Chester E. Grosch
Old Dominion University, cxgrosch@odu.edu

W. D. Thacker

Original Publication Citation

Pruett, C.D., Gatski, T.B., Grosch, C.E., & Thacker, W.D. (2003). The temporally filtered Navier-Stokes equations: Properties of the residual stress. *Physics of Fluids, 15*(8), 2127-2140. doi: 10.1063/1.1582858

The temporally filtered Navier–Stokes equations: Properties of the residual stress

C. D. Pruett
Department of Mathematics & Statistics, James Madison University, Harrisonburg, Virginia 22807

T. B. Gatski
Computational Modeling & Simulation Branch, NASA Langley Research Center, Hampton, Virginia 23681

C. E. Grosch
Departments of Ocean, Earth & Atmospheric Sciences and Computer Science, Old Dominion University, Norfolk, Virginia 23529

W. D. Thacker
Department of Physics, Parks College, Saint Louis University, St. Louis, Missouri 63156

(Received 18 September 2002; accepted 14 April 2003; published 12 June 2003)

Recent interest in the development of a unifying framework among direct numerical simulations, large-eddy simulations, and statistically averaged formulations of the Navier–Stokes equations, provides the motivation for the present paper. Toward that goal, the properties of the residual (subgrid-scale) stress of the *temporally* filtered Navier–Stokes equations are carefully examined. This includes the frame-invariance properties of the filtered equations and the resulting residual stress. Causal time-domain filters, parametrized by a temporal filter width $0<\Delta<\infty$, are considered. For several reasons, the differential forms of such filters are preferred to their corresponding integral forms; among these, storage requirements for differential forms are typically much less than for integral forms and, for some filters, are independent of Δ. The behavior of the residual stress in the limits of both vanishing and infinite filter widths is examined. It is shown analytically that, in the limit $\Delta\rightarrow 0$, the residual stress vanishes, in which case the Navier–Stokes equations are recovered from the temporally filtered equations. Alternately, in the limit $\Delta\rightarrow\infty$, the residual stress is equivalent to the long-time averaged stress, and the Reynolds-averaged Navier–Stokes equations are recovered from the temporally filtered equations. The predicted behavior at the asymptotic limits of filter width is further validated by numerical simulations of the temporally filtered forced, viscous Burger's equation. Finally, finite filter widths are also considered, and both *a priori* and *a posteriori* analyses of temporal similarity and temporal approximate deconvolution models of the residual stress are conducted for the model problem.
[DOI: 10.1063/1.1582858]

I. INTRODUCTION

The Navier–Stokes equations can be solved numerically to predict turbulent flows; however, due to the enormous computational expense required to extract a solution from these equations for flows of engineering interest, it has been necessary in most cases to revert to alternate formulations. For current purposes, three computational approaches are considered: direct numerical simulation (DNS), large-eddy simulation (LES), and Reynolds-averaged Navier–Stokes (RANS) computations. These differ primarily in the level of approximation required to achieve closure.

By definition, DNS is the numerical solution of the Navier–Stokes equations without recourse to modeling. In concept, fluid motions are resolved down to the Kolmogorov length scale. Kolmogorov theory[1] predicts the ratio of the integral scale to the Kolmogorov scale to be on the order of $\mathrm{Re}^{3/4}$, where Re is the Reynolds number based upon the integral scale. In three spatial dimensions and time, the computational requirements of DNS scale as Re^3. Consequently, for the high Reynolds number flows of engineering interest the computational requirements of fully resolved DNS are staggering. DNS at moderate Re is currently viable for certain prototypical problems such as isotropic turbulence or laminar-turbulent transition on flat plates, cylinders, and cones. For these problems, DNS plays an invaluable role both in elucidating fundamental phenomena and in serving as a yardstick to validate LES and RANS.

For LES, the separation of the field variables into resolved and unresolved (spatial) scales is effected by filtering the fields with a low-pass filter. Filtering the momentum equations generates residual (subgrid-scale) stresses that require closure either by modeling or approximation. Recent advances such as dynamic modeling[2] and deconvolution methods[3,4] have made LES practical for application to certain flows of engineering interest.[5]

Long-time averaging of the Navier–Stokes equations results in the RANS equations for the time-independent mean state. RANS methodology is generally applied to statistically steady flows. To close the system of equations, a model is needed for the Reynolds-stress tensor. Although RANS is

computationally appealing, it places a heavy burden on the Reynolds-stress model, which must incorporate the effects of all the unsteady motions upon the mean.

While the formal linkage of the LES and RANS equations has been well established,[6,7] it is of interest to investigate whether this linkage can be extended practically by developing filtering and averaging procedures that yield mutually consistent solution fields. A possible unifying context for these methodologies is afforded by filter theory. However, the linkage between LES and RANS may be more natural within the context of time-domain filtering rather than the traditional spatial filtering commonly used in LES. Accordingly, the present study focuses on the temporally filtered Navier–Stokes (TFNS) equations and the resultant residual-stress fields.

In Sec. II causal time-domain filters are discussed, and differential forms are derived for two candidate filters: an exponential filter and a Heaviside filter. The TFNS equations are formulated in Sec. III. Characteristic properties of these equations are discussed, and ancillary issues related to commutativity and frame-invariance are also addressed. Additionally, analyses of the asymptotic behaviors of the residual stress for limiting values of filter width are presented. Finally, temporal residual-stress models are proposed for the case of finite filter width. In Sec. IV, the numerical solution of the forced, viscous Burger's equation is used to validate the analytical results as well as to evaluate the proposed temporal residual-stress models by *a priori* analyses. Further validation of the proposed residual-stress models by *a posteriori* analyses is provided in Sec. V. Concluding remarks are offered in Sec. VI.

II. PROPERTIES OF TIME-DOMAIN FILTERS

Time-domain filters are classified as *causal* or *acausal*,[8] depending upon whether they are applicable to real-time or *a posteriori* data processing, respectively. The interest here lies in real-time applications for which only causal filtering is appropriate; accordingly, the focus in this study is restricted to causal filters. While aspects of time-domain filters have been discussed previously in this context,[9] it is worthwhile to reiterate some fundamental relationships for completeness.

Let $f(t)$ be a continuous function of time t. A causal linear filter is readily constructed by the integral operator

$$\overline{f}(t;\Delta)=\int_{-\infty}^{t} G(\tau-t;\Delta)f(\tau)\,d\tau, \tag{1}$$

where G is a parametrized filter kernel, and the parameter Δ is the filter width. (The convention of using semicolons to separate parameters from independent variables in argument lists is adopted here.) In general, admissible kernels must satisfy the following property:

$$G(t;\Delta)\equiv\frac{1}{\Delta}g\left(\frac{t}{\Delta}\right), \tag{2}$$

where g is any integrable function such that

$$g(t)\geqslant 0,\quad \int_{-\infty}^{0} g(t)\,dt=1,\quad g(0)=1. \tag{3}$$

The non-negativity and normalization constraints in Eq. (3) imply that

$$\lim_{t\to-\infty} g(t)=0, \tag{4}$$

and suffice for G to approach a Dirac delta function as its parameter $\Delta\to 0$; that is,

$$\lim_{\Delta\to 0}\overline{f}(t;\Delta)=\lim_{\Delta\to 0}\int_{-\infty}^{t} G(\tau-t;\Delta)f(\tau)\,d\tau$$

$$=\int_{-\infty}^{t}\delta(\tau-t)f(\tau)\,d\tau=f(t). \tag{5}$$

Two examples of simple, useful filters are obtained by use of an exponential function and a Heaviside function as kernels. For the exponential function, the kernel is

$$g(t)=\exp(t)\to G(t;\Delta)=\frac{\exp(t/\Delta)}{\Delta}, \tag{6}$$

and the resulting integral operator in Eq. (1) is

$$\overline{f}(t;\Delta)=\frac{1}{\Delta}\int_{-\infty}^{t}\exp\left(\frac{\tau-t}{\Delta}\right)f(\tau)\,d\tau. \tag{7}$$

Using the shifted Heaviside function $H(t+1)$ as $g(t)$ yields the parametrized kernel $G(t;\Delta)=(1/\Delta)H(t+\Delta)$ and the integral operator

$$\overline{f}(t;\Delta)=\frac{1}{\Delta}\int_{t-\Delta}^{t} f(\tau)\,d\tau. \tag{8}$$

The effect of a filter is most apparent from its transfer function $H(\Omega')$, which quantifies its amplitude and phase effects in Fourier space as a function of dimensionless frequency $\Omega'=\omega\Delta$. Specifically, for a causal time-domain filter

$$H(\Omega')=\int_{-\infty}^{0} G(\tau;\Delta)\exp(\iota\omega\tau)\,d\tau, \tag{9}$$

where ω is the circular frequency, and $\iota=\sqrt{-1}$. The order of a filter is associated with the flatness of the modulus of its transfer function near the origin ($\Omega'=0$). Because the exponential and Heaviside filters have zero slope but nonvanishing second derivatives at the origin, both are classified as first-order filters. However, as Fig. 1 shows, their transfer functions differ significantly away from the origin.

A drawback of the integral formulations just presented is the need to retain the long-time history of the solution field. However, by considering instead differential forms of the filter operators, storage requirements are reduced significantly, subject to the intrinsic storage needs of the numerical time-advancement scheme itself (for example, low-storage Runge–Kutta). By differentiating Eqs. (7) and (8), the differential forms of the exponential and Heaviside filters are given by

$$\frac{\partial}{\partial t}\overline{f}(t;\Delta)=\frac{f(t)-\overline{f}(t;\Delta)}{\Delta}, \tag{10}$$

and

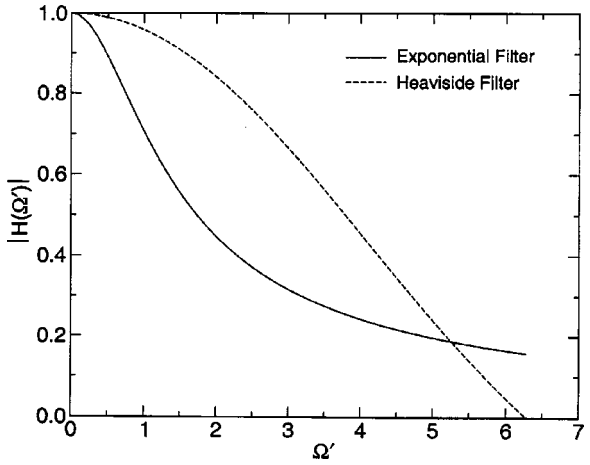

FIG. 1. Transfer functions of causal exponential and Heaviside filters.

$$\frac{\partial}{\partial t}\bar{f}(t;\Delta)=\frac{f(t)-f(t-\Delta)}{\Delta}, \tag{11}$$

respectively.

When causal filtering is applied to a temporally discretized problem with a time increment of Δt, the action of the filter is naturally parametrized by the filter-width ratio r defined as

$$r=\frac{\Delta}{\Delta t}. \tag{12}$$

For the exponential and Heaviside filters, respectively, the parametrized transfer functions are

$$H(\Omega;r)=\frac{1}{1+\imath r\Omega}, \tag{13a}$$

$$H(\Omega;r)=\frac{1-\exp(-\imath r\Omega)}{\imath r\Omega}, \tag{13b}$$

where $\Omega=\omega\Delta t$. Figure 2 shows the modulus of the transfer function of the exponential filter for selected values of the filter-width ratio. Note that $\Omega=\pi$ corresponds to a sampling rate at the Nyquist frequency, and that filtering at $\Omega>\pi$ is disallowed because it results in unacceptable aliasing error. Note also that $r=0$ yields $H(\Omega;0)=1$, which eliminates the filter.

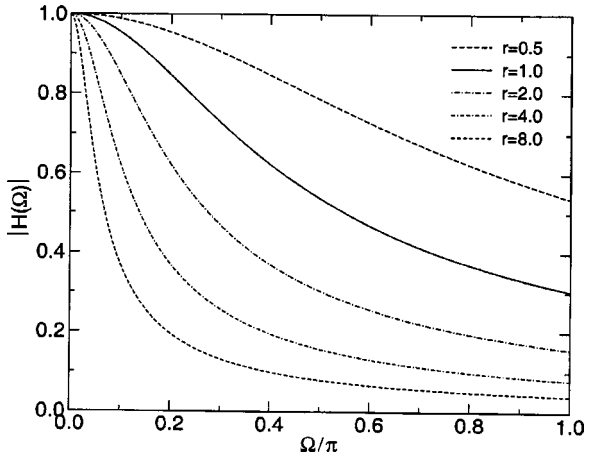

FIG. 2. Transfer function of parametrized exponential filter as a function of filter-width ratio.

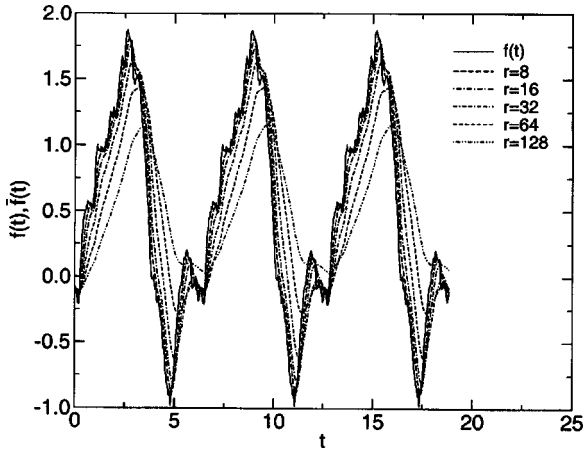

FIG. 3. Differentially filtered time series $f(t)$.

In order to illustrate the discrete differential filtering process, a 2π-periodic time series is processed by the exponential differential filter given in Eq. (10). The time series is generated from a $-3/2$ power-law decay in Fourier frequency space, and the phases are assigned randomly. The continuous signal is then sampled at a rate of 512 per period and replicated for three periods. The filtered time series, $\bar{f}$, is then generated by solving Eq. (10) from the initial condition $\bar{f}(0;\Delta)=f(0)$. There are many appropriate numerical integration schemes. Because the right-hand side of the differential form of a linear filter is itself linear, fully implicit Adams–Moulton methods are particularly attractive because of their accuracy and efficiency. Here, standard fourth-order Adams–Moulton methodology is used. The method is started with initial steps of orders one, two, and three, respectively.

The filter-width ratio, r, is the only parameter of the differential filter. In general, the larger the value of r, the more dissipative the filter. (In this context, a ''dissipative'' low-pass filter is one with significant and broad-band attenuation of high-frequency Fourier harmonics.) The method remains viable for all values of filter-width ratio $(0<r)$. For $r\approx 0$, the evolution equation becomes stiff, and small time steps are necessary. Figure 3 compares the filtered time series with the unfiltered signal for selected values of the filter-width ratio r. As r increases, the output time series becomes smoother and its amplitude diminishes due to the removal of energy at the higher frequencies. As is typical for causal filters, high levels of numerical dissipation generate significant phase lag in the output relative to the input. Figure 4 compares the input signal with the original output signal and with an output that is phase compensated by r time steps. The phase-compensated signal is an excellent representation of the input, minus its high-frequency components.

III. TEMPORALLY FILTERED NAVIER–STOKES EQUATIONS

Temporal, causal filtering of the Navier–Stokes equations using Eq. (1) leads to the following form of the TFNS equations:

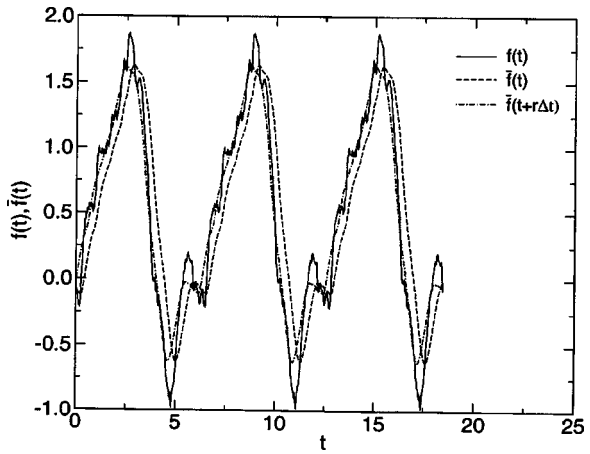

FIG. 4. Original, exponentially filtered, and phase-compensated time series $f(t)$ for $r=32$.

$$\frac{\partial \overline{u_j}}{\partial x_j}=0, \tag{14}$$

$$\frac{\partial \overline{u_i}}{\partial t}+\frac{\partial(\overline{u_i}\overline{u_j})}{\partial x_j}=-\frac{\partial \overline{p}}{\partial x_i}+\nu\frac{\partial^2 \overline{u_i}}{\partial x_j \partial x_j}-\frac{\partial[\tau_R]_{ij}}{\partial x_j}, \tag{15}$$

where u_i is the velocity, p is the pressure, and ν is the kinematic viscosity. An overbar denotes a temporal grid-filtered quantity, and $[\tau_R]_{ij}$ represents the temporal residual-stress tensor defined as

$$[\tau_R]_{ij}\equiv\overline{u_i u_j}-\overline{u_i}\,\overline{u_j}. \tag{16}$$

Provided that filtering and differentiation operations commute, the TFNS equations are *formally* identical to the spatially filtered Navier–Stokes equations. As pointed out previously by Pruett,[9] commutativity is natural for temporal filters but remains problematic for spatial ones.[10,11] It is now recognized[12–14] that this formal equivalence does *not* imply quantitative equivalence of the residual-stress fields. In general, for spatial *or* temporal grid filters, the residual stress depends strongly upon the filter, particularly upon its filter width and order property, which influence both the magnitude and the distribution of the residual stress. The implication of this growing awareness is that the residual-stress model cannot be independent of the choice of the filter. To make explicit its formal dependence upon the specific temporal filter, the residual stress is denoted by $[\tau_R]_{ij}(\Delta)$ where appropriate.

Before examining the effect of the filter width Δ on the behavior of the residual stress, it is useful to establish some of the frame-invariance properties of both the TFNS equations and the temporal residual stress $[\tau_R]_{ij}$.

A. Frame-invariance properties

It has been shown previously[9] that the TFNS equations are frame invariant under the Galilean group of transformations. In order to further explore the range of applicability as well as limits of the TFNS formulation, it is useful to examine the frame-invariance properties of the TFNS under the more general Euclidean group of transformations.

Examining the transformation properties of the Navier–Stokes equations even under the Euclidean group is relatively straightforward and the various forms of the equations in the noninertial frames are well known. However, when temporal filtering of the variables as well as the governing equations is involved, care must be exercised in order to obtain the proper relations and interpretation of the results. This is due to the fact that the direction cosines Q_{ij} of the transformation are time dependent and as such become necessarily coupled to and inseparable from the flow variables under the filtering process.

In order to properly interpret the results of the transformations, it is necessary to identify the frame of reference that serves as the base Eulerian system, that is, the frame in which the observer is fixed. Consider the rectangular coordinates x_i^* of a point in a frame of reference in arbitrary time-dependent motion (rotation and translation) relative to an inertial frame with corresponding coordinates x_i. In the first case, the observer is fixed in the inertial frame. Under the Euclidean group, the spatial coordinates and corresponding velocity field then transform as

$$x_i^*(t^*)=Q_{ij}[x_j+b_j], \tag{17a}$$

$$u_i^*(t^*,x_k^*)=\dot{Q}_{ij}[x_j+b_j]+Q_{ij}[u_j+\dot{b}_j], \tag{17b}$$

where $\mathbf{Q}=\mathbf{Q}(t)$ is a time-dependent proper orthogonal tensor ($\mathbf{QQ}^T=\mathbf{I}$, $\det \mathbf{Q}=+1$, $\mathbf{I}$ is the identity tensor), $(\dot{})$ denotes the time derivative, and $b_j=b_j(t)$ is any time-dependent vector with $t^*=t+t_0$ (t_0 is an arbitrary constant time shift). The temporal filter widths in the respective frames are unaffected ($\Delta^*=\Delta$) by such transformations and do not need to be considered explicitly in the remainder of the frame-invariance discussion. In this case, to an observer in the inertial frame, the spatial coordinates in the noninertial frame vary with time; whereas, the spatial coordinates in the inertial Eulerian frame are fixed.

In the second case, the observer is fixed in the noninertial frame. Under the Euclidean group, the spatial coordinates and corresponding velocity field then transform as

$$x_j(t)=Q_{ij}x_i^*-b_j, \tag{18a}$$

$$u_j(t,x_k)=Q_{ij}u_i^*+\dot{Q}_{ij}x_i^*-\dot{b}_j. \tag{18b}$$

In this case, to an observer in the noninertial frame, the spatial coordinates in the inertial frame vary with time; whereas, the spatial coordinates in the noninertial Eulerian frame are fixed. With this background, the frame-invariant questions pertinent to the properties of the filtered and residual variables as well as the TFNS equations in the noninertial frame x_i^* can be addressed.

For the case where the inertial frame is the Eulerian frame, the transformation properties of the filtered spatial coordinates and filtered velocity fields can be written as

$$\overline{x_i^*}=\overline{Q}_{ij}x_j+\overline{Q_{ij}b_j}, \tag{19a}$$

$$\overline{u_i^*}(t^*,x_k^*)=\overline{\dot{Q}_{ij}[x_j+b_j]}+\overline{Q_{ij}[u_j+\dot{b}_j]}, \tag{19b}$$

where $\overline{x_j}=x_j$ for the (inertial) Eulerian system. For the case where the noninertial frame is the Eulerian frame, the transformation properties of the filtered spatial coordinates and filtered velocity fields can be written as

$$\overline{x_j}=\overline{Q}_{ij}x_i^*-\overline{b}_j, \tag{20a}$$

$$\overline{u_j}=\overline{Q_{ij}u_i^*}+\overline{\dot{Q}_{ij}}x_i^*-\overline{\dot{b}_j}, \tag{20b}$$

where $\overline{x_i^*}=x_i^*$ for the (noninertial) Eulerian system.

It is easily seen from Eqs. (19b) and (20b) that the filtered velocity fields are not frame invariant under a Euclidean transformation—a result consistent with that obtained for the (spatial filtered) LES approach.[15] However, due to the inseparable coupling of the direction cosines Q_{ij} with the velocity field, the filtered velocity field does not transform in the same manner as the unfiltered velocity field—a result that contrasts with that obtained for the (spatial filtered) LES approach.[15] For the subset group of Galilean transformations, where Q_{ij} is time independent and $b_j=-V_jt$ (V_j are constant components of a translational velocity imposed on the noninertial frame),[16] the filtered velocity field transforms in the same way as the unfiltered velocity—a result consistent with the (spatial filtered) LES approach,[17] but in contrast to a result arrived at in a previous study.[9]

The next question to address is the transformation properties of the residual fields. These fields are the differences between the instantaneous and filtered fields. For the case where the Eulerian frame is the inertial frame, Eqs. (17b) and (19b) yield

$$\tilde{u}_i^*=u_i^*-\overline{u_i^*}=[Q_{ik}u_k-\overline{Q_{ik}u_k}]+[\dot{Q}_{ik}-\overline{\dot{Q}_{ik}}]x_k +[(\dot{Q_{ik}}b_k)-\overline{(\dot{Q_{ik}}b_k}, \tag{21a}$$

and for the case where the Eulerian frame is the noninertial frame, Eqs. (18b) and (20b) yield

$$\tilde{u}_j=u_j-\overline{u_j}=[Q_{kj}u_k^*-\overline{Q_{kj}u_k^*}] +[\dot{Q}_{kj}-\overline{\dot{Q}_{kj}}]x_k^*-[\dot{b}_j-\overline{\dot{b}_j}]. \tag{21b}$$

A comparison of Eqs. (21a) and (21b) shows that the residual velocity field is not frame-invariant under the Euclidean group—a result that contrasts with that obtained for the (spatial filtered) LES approach.[15] However, as will be shown in the following, for the Galilean group the residual velocity field is frame-invariant.

The final transformation property under the Euclidean group to be addressed is the form of the TFNS equations in the noninertial frame. As is well known, the Navier–Stokes equations are not frame-invariant under the Euclidean group since in a noninertial frame they take the form

$$\frac{Du_i^*}{Dt^*}=\frac{\partial u_i^*}{\partial t^*}+u_k^*\frac{\partial u_i^*}{\partial x_k^*}=-\frac{\partial P^*}{\partial x_i^*}+\nu\frac{\partial^2 u_i^*}{\partial x_k^*\partial x_k^*}+2\Omega_{ik}u_k^* +\dot{\Omega}_{ik}x_k^*, \tag{22a}$$

with a modified pressure P^* (that includes both the centrifugal acceleration and the translational acceleration) given by

$$P^*=p^*+\tfrac{1}{2}\Omega_{kl}\Omega_{ln}x_n^*x_k^*-Q_{nk}\ddot{b}_k^*x_n^*, \tag{22b}$$

where the rotation rate tensor Ω_{ij} represents the angular velocity of the noninertial frame relative to the inertial frame and is defined by

$$\Omega_{ik}\equiv\dot{Q}_{il}Q_{kl}. \tag{23}$$

Since $\ddot{b}_n$ is frame invariant, the (objective) transformation $\ddot{b}_k^*=Q_{kn}\ddot{b}_n$ has been used in Eq. (22b). [Note that Eq. (22) can be derived directly starting with the transformation properties described in Eq. (18).] The question now is: For an observer fixed in the noninertial Eulerian frame, what form do the TFNS equations take under the Euclidean transformation group? These equations can be obtained by first taking the material derivative of Eq. (17b) and then filtering

$$\overline{\frac{Du_i^*}{Dt^*}}=-\overline{\ddot{Q}_{kl}Q_{il}}x_k^*-2\overline{\dot{Q}_{kl}Q_{il}u_k^*}+\overline{Q_{ij}\frac{Du_j}{Dt}}+\overline{Q_{ij}\ddot{b}_j} =\overline{(\dot{\Omega}_{ik}-\Omega_{il}\Omega_{lk})}x_k^*+2\overline{\Omega_{ik}u_k^*}+\overline{Q_{ij}\frac{Du_j}{Dt}}+\overline{Q_{ij}\ddot{b}_j}, \tag{24a}$$

where the Navier–Stokes equations in the inertial frame are used to obtain

$$\overline{Q_{ij}\frac{Du_j}{Dt}}=-\overline{Q_{ij}\frac{\partial p}{\partial x_j}}+\nu\overline{Q_{ij}\frac{\partial^2 u_i}{\partial x_k\partial x_k}}=-\frac{\partial\overline{p^*}}{\partial x_i^*}+\nu\frac{\partial^2\overline{u_i^*}}{\partial x_k^*\partial x_k^*}. \tag{24b}$$

Introducing the residual stress into the formulation, Eq. (24a) can then be written in the form

$$\frac{\partial\overline{u_i^*}}{\partial t^*}+\overline{u_k^*}\frac{\partial\overline{u_i^*}}{\partial x_k^*} =-\frac{\partial\overline{P^*}}{\partial x_i^*}+\nu\frac{\partial^2\overline{u_i^*}}{\partial x_k^*\partial x_k^*}+2\overline{\Omega_{ik}u_k^*}+\overline{\dot{\Omega}_{ik}}x_k^*-\frac{\partial[\tau_R]_{ik}^*}{\partial x_k^*}, \tag{25a}$$

where

$$\overline{P^*}=\overline{p^*}+\tfrac{1}{2}\overline{\Omega_{kl}\Omega_{ln}}x_n^*x_k^*-\overline{\ddot{b}_k^*}x_k^*, \tag{25b}$$

and

$$[\tau_R]_{ik}^*=\overline{u_i^*u_k^*}-\overline{u_i^*}\ \overline{u_k^*}. \tag{25c}$$

It is clear from a comparison between Eqs. (22) and (25) that the TFNS do not in general retain the same form as the Navier–Stokes equations in the noninertial frame under the Euclidean group—a result that contrasts with that obtained for the (spatial filtered) LES approach.[15] The differences lie in the form of the Coriolis and centrifugal acceleration terms, as well as the rotational acceleration term. The Coriolis acceleration is the most significantly affected due to the inseparable coupling with the velocity field brought about by the temporal filtering process. For the important case of constant rotation rate Ω_{ij} and nonaccelerating translational frames, Eq. (25) can be written in the form

$$\frac{\partial \overline{u_i^*}}{\partial t^*}+\overline{u_k^*}\frac{\partial \overline{u_i^*}}{\partial x_k^*}=-\frac{\partial \overline{P^*}}{\partial x_i^*}+\nu\frac{\partial^2 \overline{u_i^*}}{\partial x_k^* \partial x_k^*} +2\Omega_{ik}\overline{u_k^*}-\frac{\partial [\tau_R]_{ik}^*}{\partial x_k^*}, \tag{26a}$$

where

$$\overline{P^*}=\overline{p^*}+\tfrac{1}{2}\Omega_{kl}\Omega_{ln}x_n^* x_k^*. \tag{26b}$$

In this case, the TFNS equations retain the same form as the Navier–Stokes equations in the noninertial frame.

As the TFNS equations show, the residual stress $[\tau_R]_{ik}^*$ given in Eq. (25c) is defined in the same manner as its inertial frame counterpart. Nevertheless, models developed for the residual stress field will suffer from the same deficiencies as the residual velocity field under the Euclidean group. The reason, stated previously, is the unavoidable coupling between the time-dependent relative motion of the frames and the time-dependent flow field. From a modeling standpoint, models for $[\tau_R]_{ik}^*$ developed for inertial frames may not suffice in the noninertial frames and will have to be modified to account for the noninertial effects. This is neither surprising nor uncommon, because turbulent flow models routinely account for such rotational effects.

The analysis to this point has been rather general and necessarily detailed. To bring the section to a close, it is worthwhile to limit the discussion to the more familiar Galilean group of transformations where the frame-invariance properties are, in general, consistent with spatial filtered LES results. Inspection of Eqs. (17b) and (21) shows that under the Galilean group (Q_{ij} and $\dot{b}_j=-V_j$ constant), both the filtered velocity and unresolved velocity consistently transform and are given by

$$\overline{u_i^*}=Q_{ij}[\overline{u_j}+V_j], \quad \tilde{u}_i^*=Q_{ij}\tilde{u}_j. \tag{27}$$

Thus, the unresolved velocity field $\tilde{u}_i$ as well as the filtered unresolved velocity field are frame indifferent under the Galilean group. With these properties for both the filtered and unresolved velocity fields, it can also be shown that the residual stress $[\tau_R]$ is now frame invariant, so that

$$[\tau_R]_{ij}^*=Q_{ik}Q_{jl}[\tau_R]_{kl}. \tag{28}$$

The Galilean transformation properties established for the temporal filtering process are similar to those established for the spatial filtering process.[17] This group invariance of the TFNS equations and the residual stress given by Eq. (28) shows that the evolution of the filtered scales of motion is the same. In addition, this result will be used in Sec. III B to further validate the equivalence of the residual stress and the long-time averaged stress in the limit of infinite filter width.

B. Limiting behaviors

Of interest in this section is the effect of filter width Δ on the residual stress $[\tau_R]_{ij}$. It is easily shown that the $[\tau_R]_{ij}$ vanishes in the limit $\Delta\to 0$. In this limit, the kernel function reduces to a Dirac delta function [see Eq. (5)] so that

$$\lim_{\Delta\to 0}[\tau_R]_{ij}(t,x;\Delta)=\lim_{\Delta\to 0}(\overline{u_iu_j}-\overline{u_i}\,\overline{u_j})=(u_iu_j-u_iu_j)=0. \tag{29}$$

The vanishing of the temporal residual stress, coupled with the replacement of the other filtered quantities by their unfiltered counterparts, leads to the recovery of the Navier–Stokes equations from the TFNS equations in the limit $\Delta\to 0$.

The other limit of interest is $\Delta\to\infty$. However, before examining the behavior of the residual stress in this limit, it is useful to examine some characteristics of the filtered velocity field itself. It follows from the differential forms of either the exponential or Heaviside differential filters given in Eq. (10) or (11) that

$$\lim_{\Delta\to\infty}\frac{\partial \overline{u_i}}{\partial t}(t,x;\Delta)=0, \tag{30}$$

where both u_i and $\overline{u_i}$ are assumed bounded. The above-mentioned condition establishes that $\overline{u_i}(t,x;\infty)$ is actually independent of time t. [In fact, for Eq. (30) to hold, it suffices that u_i is bounded and that $|g'(t)|$ is integrable on $(-\infty,0]$.] Thus, Eq. (30) applies to a wide class of filters. For the causal temporal filter defined in Eq. (1) with the Heaviside kernel (for convenience), $\overline{u_i}(t,x;\infty)$ can be written as

$$\lim_{\Delta\to\infty}\overline{u_i}(t,x;\Delta)=\overline{u_i}(0,x;\infty)=\lim_{\Delta\to\infty}\frac{1}{\Delta}\int_{-\Delta}^{0}u_i(\tau,x)\,d\tau. \tag{31}$$

Equation (31) holds for any filter for which $H(0)=1$, which is typical of low-pass filters. The right-hand side of Eq. (31) simply defines the long-time average of the variable $u_i(t,x)$, which, for a stationary process, is equivalent to the ensemble average according to the ergodic hypothesis. That is, for a stationary flow

$$\overline{u_i}(0,x;\infty)=E\{u_i(t,x)\}, \tag{32}$$

where $E\{\}$ denotes the expected value (or ensemble average). However, Eq. (30) has shown that $\overline{u_i}(t,x;\infty)$ is constant with respect to time so that

$$\overline{u_i}(t,x;\infty)=\overline{u_i}(0,x;\infty)=E\{u_i(t,x)\}=U_i(x), \tag{33}$$

and

$$\lim_{\Delta\to\infty}\frac{\partial}{\partial t}\overline{u_i}(t,x;\infty)=\frac{\partial}{\partial t}E\{u_i(t,x)\}=0. \tag{34}$$

In the current time-filtered approach, Eq. (33) provides the link between the resolved motions of the variable $u_i(t,x)$ and the ensemble mean $U_i(x)$. Because the variable $u_i(t,x)$ can be partitioned either into a sum of resolved $\overline{u_i}(t,x;\infty)$ and temporally unresolved motions $\tilde{u}_i(t,x)$, or into a sum of time mean $U_i(x)$ and fluctuating $u_i'(t,x)$ quantities, it follows from Eq. (33) that

$$\tilde{u}_i(t,x;\infty)=u_i'(t,x). \tag{35}$$

In addition to the equality between the resolved and mean fields in the limit, Eq. (35) shows the linkage between the

temporally unresolved and fluctuating motions. With these results, it is now possible to examine the limiting behavior of the residual stress.

By the linearity of the filter operator, the residual stress defined in Eq. (16) can be written as

$$\lim_{\Delta\to\infty}[\tau_R]_{ij}(\Delta)=\lim_{\Delta\to\infty}[(\overline{\overline{u_i}\overline{u_j}}+\overline{\overline{u_i}\widetilde{u}_j}+\overline{\widetilde{u}_i\overline{u}_j}+\overline{\widetilde{u}_i\widetilde{u}_j})-\overline{u_i}\,\overline{u_j}], \tag{36}$$

where the instantaneous velocity field has been partitioned into resolved and unresolved parts. Because Eqs. (32) and (33) establish an equality between the resolved and ensemble mean fields, and the residual and fluctuating fields, respectively, Eq. (36) can be simplified to

$$\lim_{\Delta\to\infty}[\tau_R]_{ij}(\Delta)=E\{u_j'E\{u_i\}+u_i'E\{u_j\}+u_i'u_j'\}$$

$$=E\{u_i'u_j'\}=\tau_{ij}. \tag{37}$$

That is, for a stationary flow the residual stress ($[\tau_R]_{ij}$) asymptotically approaches the Reynolds stress (τ_{ij}) as $\Delta\to\infty$. It is well known[16] that the long-time averaged stress is Galilean invariant. As was shown in Eq. (28), the residual stress also retains this feature, which further validates the equivalence of the two stress fields established in Eq. (37).

C. Finite filter width

For finite filter width, the residual stress represents the dynamics of a broad spectral range of motions. The TFNS equations provide a governing set of equations suitable for time-filtered LES[9] (or TLES), for which (accurate) modeling of $[\tau_R]_{ij}$ is required for closure.

The temporal variants of two well-known residual-stress models for $[\tau_R]_{ij}$ are considered: Bardina's scale-similarity model[18] (SSM); and the approximate deconvolution model (ADM) of Stolz and Adams.[4] The time-filtered counterparts of these models are referred to as the temporal scale-similarity model (TSSM) and the temporal approximate deconvolution model (TADM), respectively.

Consider first a TSSM that is formally equivalent to the Bardina model,[18]

$$[\tau_R]_{ij}\approx\overline{\overline{u_i}\overline{u_j}}-\bar{\bar{u}}_i\bar{\bar{u}}_j \quad \text{(TSSM)}. \tag{38}$$

As in the Bardina model, the same (temporal) filter width is used for the primary and secondary (test) filters. Next, the TADM considered is formally equivalent to the second of the ADM models presented by Stolz and Adams,[4]

$$[\tau_R]_{ij}\approx\overline{v_iv_j}-\overline{v}_i\overline{v}_j \quad \text{(TADM)}, \tag{39}$$

where v_i is an approximate deconvolution of $\overline{u}_i$; that is, v_i approximates u_i based upon approximately defiltering (deconvolving) $\overline{u}_i$. Following Stolz and Adams, the zeroth- and first-order deconvolutions of $\overline{u}_i$ yield $v_i=\overline{u}_i$ and $v_i=2\overline{u}_i-\bar{\bar{u}}_i$, respectively. Higher-order (and more accurate) deconvolutions are possible. Note that the TADM (ADM) generalizes the TSSM (SSM), because the zeroth-order deconvolution is the TSSM. (Appropriately, Stolz and Adams[4] refer to the second of their ADM models as the generalized SSM model.) Consequently, we use the single nomenclature $[\tau_R]_{\text{mod}}$ for both models. It should be noted that the temporal residual-stress models given in Eqs. (38) and (39) are frame-indifferent under Galilean transformations; a property that the exact residual stress has been shown in Eq. (28) to have.

In Sec. IV, an *a priori* analysis of the predictive capability of these two residual-stress models will be performed.

IV. FORCED VISCOUS BURGER'S EQUATION

While it is desirable and ultimately necessary to validate the analytical results previously established in simulations of the full TFNS equations, the wide range of parameter values considered here renders such analyses cost prohibitive. However, it is possible to illustrate the dependence of the residual stress upon the temporal filter width, in general, and the asymptotic behaviors discussed previously, in particular, by simulations of a spatially one-dimensional model problem. To this end, consider the forced, viscous Burger's equation (VBE), written in the form

$$\frac{\partial u}{\partial t}+\frac{1}{2}\frac{\partial(u^2)}{\partial x}=\nu\frac{\partial^2u}{\partial x^2}+F(t,x) \quad (0<x<2\pi), \tag{40}$$

with $u(t,x)$ a velocity, $F(t,x)$ an imposed forcing function, and ν a viscosity. The initial condition is $u(0,x)=1$. Without forcing, the initial condition results in a velocity field that is constant for all time and space. Moreover, any perturbations of that field decay toward zero, so that constant "stirring" is required to maintain high-intensity fluctuations.[19] This equation can be solved accurately by a Galerkin Fourier spectral method in space coupled with classical fourth-order Runge–Kutta (RK4) time advancement. A Fourier *ansatz* is assumed for u and substituted into the governing equation. This results in a system of coupled ordinary differential equations for the complex Fourier coefficients U_k, $k=-n/2,...,-1,0,+1...,+n/2$. (Due to conjugate symmetry, only $n/2+1$ nonnegative modes are solved for explicitly.) The equations are coupled through their nonlinear terms, which are evaluated exactly in Fourier space by Cauchy products. Hence, explicit de-aliasing is unnecessary.

For this forced case, $n=256$, and each Fourier mode in the band $1\leqslant k\leqslant k_F$ is independently subjected to periodic forcing $F_k(t)$ such that $F_k(t)=A\phi_k\exp(\iota\omega_kt)$ with real frequency $\omega_k=k\omega$. The band limit $k_F=32$, the fundamental frequency $\omega=1$, and the amplitude $A=0.4$ (the same for all modes) are input parameters, and the time increment is 0.005 throughout. The complex phases $\phi_k=\exp(\iota\alpha_k)$ are assigned initially by random numbers α_k uniformly distributed on $[0,2\pi]$. Thereafter, they remain fixed. As will be shown, after a long-time evolution, a statistically steady flow results. Because, at small ν, the viscous Burger's equation admits solutions with steep shock fronts, only a moderately large value of ν is practical. For the value $\nu=1/300$ and forcing distribution, the flow is highly resolved in both time and space, with Fourier amplitudes at the highest wavenumbers of less than 10^{-10}.

Causally filtering the forced VBE results in the following equation, which can be considered as a one-dimensional analog of the TFNS equation given in Eq. (15):

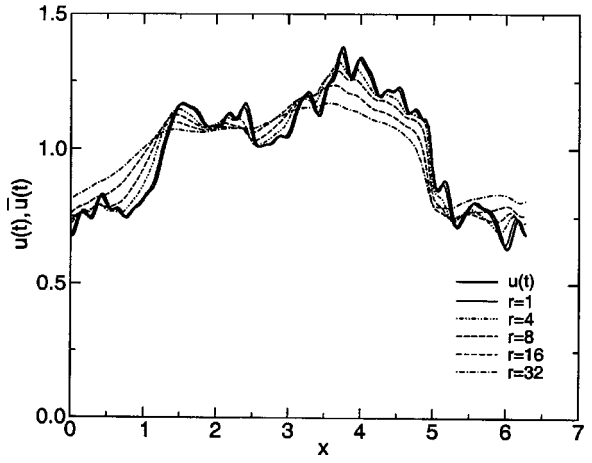

FIG. 5. Instantaneous and causally filtered velocity fields at $t=10$ for filter-width ratios $r=1$, $r=4$, $r=8$, $r=16$, and $r=32$.

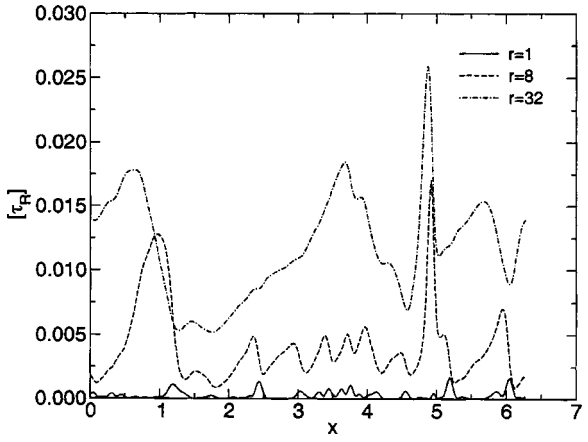

FIG. 6. Instantaneous residual stress $[\tau_R]$ at $t=10$ for filter-width ratios $r=1$, $r=8$, and $r=32$.

$$\frac{\partial \overline{u}}{\partial t}+\frac{1}{2}\frac{\partial(\overline{uu})}{\partial x}=\nu\frac{\partial^2\overline{u}}{\partial x^2}+\overline{F}(t,x)-\frac{1}{2}\frac{\partial[\tau_R]}{\partial x}$$

$$(0<x<2\pi). \tag{41}$$

Filtering generates a residual stress given by

$$[\tau_R]=\overline{uu}-\overline{u}\,\overline{u}. \tag{42}$$

In Fig. 5, the instantaneous unfiltered velocity field, obtained from the solution of Eq. (40) at $t=10$ ($\Delta t=0.005$), is compared with the filtered field, which satisfies Eq. (41), for selected values of the filter-width ratio r. Clearly, filtering in time to remove high frequencies effects the removal of energy at high wavenumbers as well.

As implied in Sec. III B, the behaviors of the residual stress for limiting values of the temporal filter width Δ are key results of the temporally filtered methodology being studied. To illustrate these predicted behaviors in the limits $\Delta\to 0$ and $\Delta\to\infty$, the model problem is particularly useful.

A. Limiting behavior of exact residual stress

The behavior in the limit $\Delta\to 0$ can be verified numerically by using successively smaller temporal grid-filter widths to process the numerical solution $u(t,x)$ of the VBE. The exact residual stress (42) is evaluated to the accuracy of the numerical scheme by solving, in addition to Eq. (40), the filter evolution equations [cf. Eq. (10)]

$$\frac{\partial \overline{u}}{\partial t}=\frac{u-\overline{u}}{\Delta}, \tag{43a}$$

$$\frac{\partial \overline{uu}}{\partial t}=\frac{uu-\overline{uu}}{\Delta} \tag{43b}$$

from initial conditions $\overline{u}(0,x)=u(0,x)$ and $\overline{uu}(0,x)=u^2(0,x)$. Here, these equations (43) are advanced in time using the standard fourth-order Adams–Moulton method. (The fourth-order Runge–Kutta methodology used to advance the VBE would also be suitable for all the filter equations; however, following the Runge–Kutta update of the solution by the fourth-order Adams–Moulton updates of the filtered quantities has the algorithmic advantage of compartmentalizing the code.) While Eq. (43) applies to the exponential filter, an analogous set could be derived for the Heaviside filter.

Figure 6 compares the exact, instantaneous residual stress $[\tau_R]$ at $t=10$ determined from Eqs. (40) and (43) for selected values of the filter-width ratio $r(=\Delta/\Delta t)$. As expected, the amplitude envelope of the residual stress tends toward zero as r decreases.

The behavior of the velocity and residual stress fields in the limit of $\Delta\to\infty$ can also be analyzed. As was shown in Sec. III B, the limiting form of the residual stress $[\tau_R]$ approaches the long-time average stress field τ. While this can be shown by considering successively larger values of the filter-width ratio r, it is first necessary to establish that the solution of the forced, viscous Burger's equation evolves to a statistically steady (stationary) state. Thus, it is necessary to verify the stationarity of the numerical solution, because the equality of the residual stress and Reynolds stress in the long-time limit is based on this assumption. [See Eqs. (33) and (34).]

The long-time average and the spatial average of the instantaneous velocity field $u(t,x)$ are both equal to unity. The fluctuating field $u'(t,x)$ is extracted at each time step simply by subtracting this mean value from $u(t,x)$. To verify that the (long-time) solution of the forced viscous Burger's equation is indeed stationary, a variety of statistical quantities are analyzed. These include the fluctuating intensity $u'_{\rm rms}(=\sqrt{\langle u'^2\rangle_t})$, energy dissipation rate $\epsilon=(2\nu\langle(du'/dx)^2\rangle_t)$, skewness $(=\langle u'^3\rangle_t/\langle u'^2\rangle_t^{3/2})$, and kurtosis $(=\langle u'^4\rangle_t/\langle u'^2\rangle_t^2)$. These statistics were obtained from windowed time averages of the time-varying field $u'(t,x)(=u(t,x)-\langle u(t,x)\rangle_t)$, with $\langle u(t,x)\rangle_t=(1/\Delta)\int_{t-\Delta}^{t}u(\tau,x)d\tau$. (Such windowed averages are equivalent to *ex post facto* filtering with the Heaviside filter, albeit for very large Δ.) Figures 7, 8, and 9 present these averages for window-width ratios of $r=250$, $r=1000$, and $r=4000$, respectively. Slight variations in the x direction have been eliminated by simply averaging over the domain length. It appears that, after an initial transient period $0\leqslant t\leqslant 200$, the flow is stationary on a time scale of approximately

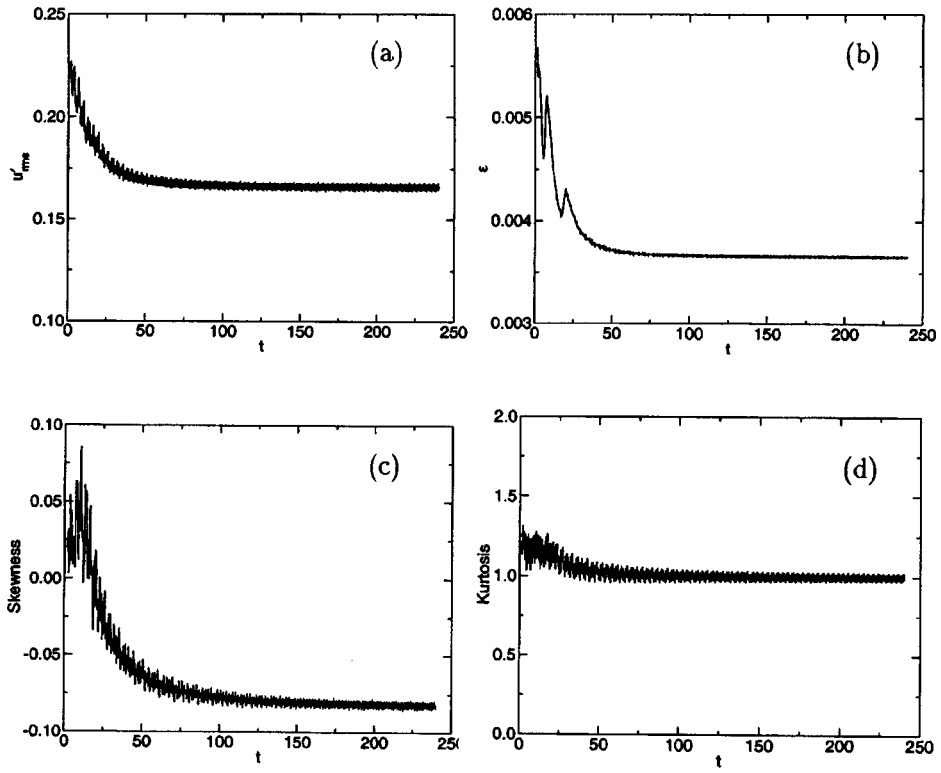

FIG. 7. Window-averaged turbulence quantities for $r=250$: (a) root-mean-square velocity u'_{rms}, (b) energy dissipation rate ϵ, (c) skewness, (d) kurtosis.

$\Delta=20$ ($r=4000$). In addition, for sufficiently large temporal windows Δ, it was found that the statistical quantities are virtually independent of x as well, suggesting that the solution is also statistically homogeneous.

Now that the stationarity of the solution of the forced VBE has been established, it is possible to evaluate the effect of large filter width on the residual stress. In Fig. 10 the long-time averaged stress τ is compared with the instantaneous residual stress $[\tau_R](\Delta)$ at $t=240$ for different values of the filter-width ratio r. The stress τ is computed by averaging over an interval of duration $\Delta=20$ during the period in which the flow is essentially stationary ($t=240-260$). As expected, the residual stress $[\tau_R]$, computed in real time using the exponential filter, appears to converge toward the

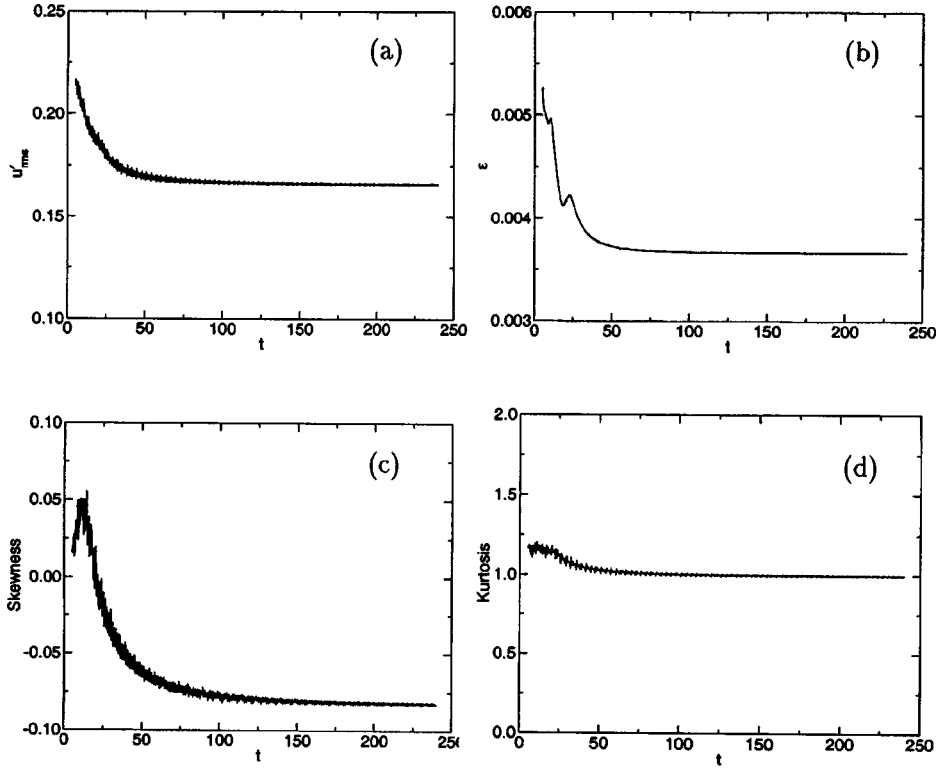

FIG. 8. Window-averaged turbulence quantities for $r=1000$: (a) root-mean-square velocity u'_{rms}, (b) energy dissipation rate ϵ, (c) skewness, (d) kurtosis.

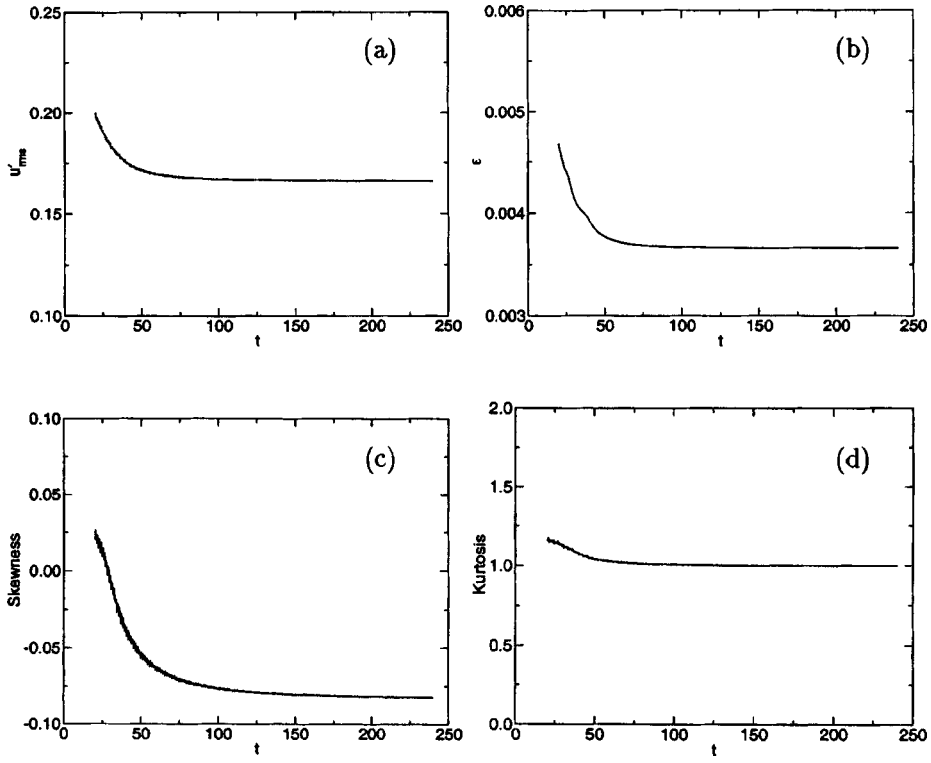

FIG. 9. Window-averaged turbulence quantities for $r=4000$: (a) root-mean-square velocity u'_{rms}, (b) energy dissipation rate ϵ, (c) skewness, (d) kurtosis.

value of τ as Δ becomes large. Moreover, a further indication of convergence is that the spatial averages of the residual stress (that is, $\langle[\tau_R]\rangle_x$), provided in the legend of Fig. 10, tend rapidly toward the value of τ ($=0.0185$) as the filter-width ratio r increases.

B. Residual stress for finite filter width

With the limiting behavior of the filter-width Δ on $[\tau_R]$ established for the forced VBE, it remains only to evaluate the behavior of $[\tau_R]$ for finite filter width. As described previously, the exact residual stress is extracted from the solutions of Eqs. (40) and (43). The modeled residual stress can be obtained from these equations by further appending the evolution equations

$$\frac{\partial \bar{\bar{u}}}{\partial t}=\frac{\bar{u}-\bar{\bar{u}}}{\Delta}, \tag{44a}$$

$$\frac{\partial \overline{\overline{uu}}}{\partial t}=\frac{\overline{uu}-\overline{\overline{uu}}}{\Delta}, \tag{44b}$$

and

$$\frac{\partial \bar{v}}{\partial t}=\frac{v-\bar{v}}{\Delta}, \tag{45a}$$

$$\frac{\partial \overline{vv}}{\partial t}=\frac{vv-\overline{vv}}{\Delta}. \tag{45b}$$

Equation (44) is used in conjunction with the TSSM, subject to the initial conditions $\bar{\bar{u}}(0,x)=u(0,x)$ and $\overline{\overline{uu}}(0,x)=u^2(0,x)$. For the TADM, both sets, Eqs. (44) and Eqs. (45) are involved, subject to the additional initial conditions $\bar{v}(0,x)=u(0,x)$ and $\overline{vv}(0,x)=u^2(0,x)$. As before, these differential filter equations are advanced by the Adams–Moulton method.

In Fig. 11, the exact ($[\tau_R]$) and modeled ($[\tau_R]_{\mathrm{mod}}$) residual stresses are compared at $t=20$. Because the TSSM is a degenerate case of the TADM, the following definition suffices for both models:

$$[\tau_R]_{\mathrm{mod}}=\overline{vv}-\overline{vv}, \tag{46}$$

where v is an approximate deconvolution of $\bar{u}$. At this instant, the flow statistics are still evolving in time, for in the

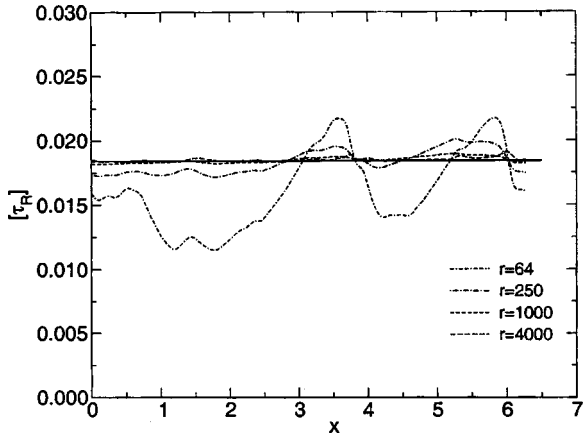

FIG. 10. Instantaneous residual stress $[\tau_R]$ at $t=240$ for selected values of filter-width ratio r: (—) long-time stress τ. Moreover, spatial averages of $[\tau_R](=\langle[\tau_R]\rangle_x)$ are 0.0161 ($r=64$), 0.0183 ($r=250$), 0.0185 ($r=1000$), and 0.0185 ($r=4000$), relative to $\tau=0.0185$.

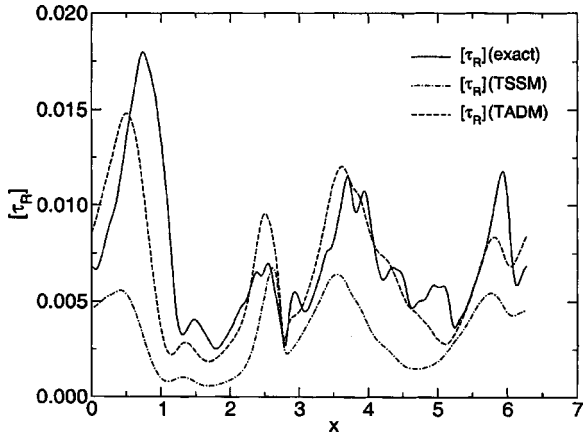

FIG. 11. Instantaneous exact and modeled (TSSM, TADM) residual stresses ($[\tau_R]$) at $t=20$.

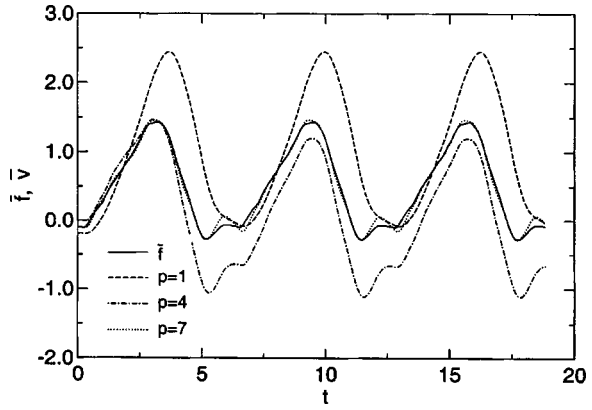

FIG. 13. Filtered deconvolutions $\bar{v}$ of selected orders compared with filtered time-series $\bar{f}$. Signal $f(t)$ is that of Fig. 3, and $r=64$.

finite-Δ case, there is no reason to presuppose stationarity. A fairly dissipative filter of ratio $r=16$ is used for the *a priori* analysis. Note that for both the exact and modeled residual stresses, $[\tau_R]>0$ at all times. This realizability property[20] is a consequence of the positivity of the filter kernel established in Eq. (3).

In order to quantify the fidelity of the models, a time-dependent correlation coefficient, C, is computed for the time interval of interest, $20\leqslant t\leqslant 40$. Specifically

$$C([\tau_R],[\tau_R]_{\mathrm{mod}}) = \frac{\langle[\tau_R][\tau_R]_{\mathrm{mod}}\rangle_x-\langle[\tau_R]\rangle_x\langle[\tau_R]_{\mathrm{mod}}\rangle_x}{[(\langle[\tau_R]^2\rangle_x-\langle[\tau_R]\rangle_x^2)(\langle[\tau_R]_{\mathrm{mod}}^2\rangle_x-\langle[\tau_R]_{\mathrm{mod}}\rangle_x^2)]^{1/2}}, \tag{47}$$

where the spatial average over the 2π length in the x direction is $\langle u(t,x)\rangle_x=(1/2\pi)\int_0^{2\pi}u(t,x')dx'$. Figure 12 presents the (optimally phase-compensated) correlations over the interval of interest. Both the TSSM and TADM correlate relatively well with $[\tau_R]$, with correlation coefficients on the order of 0.8 and 0.9, respectively. Correlations, however, reflect distribution but not amplitude. In general, the TADM has a higher correlation, and its amplitude tends to be more nearly correct. That the TADM performs well with only first-order deconvolution is surprising (as Stolz and Adams[4] employ fifth order). It is important to note that the classical Smagorinsky model widely used in LES typically correlates at less than 20% against exact residual stress.[21,22]

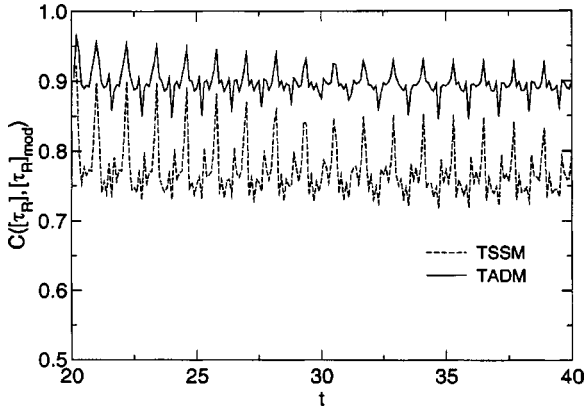

FIG. 12. Optimally phase-compensated correlations between exact and modeled residual stress as functions of time.

C. Limiting behavior of modeled residual stress

Finally, we consider the behavior of the models TSSM [Eq. (38)] and TADM [Eq. (39)] in the limits $\Delta\to 0$ and $\Delta\to\infty$. By virtue of Eq. (5), both models vanish appropriately, as does the exact residual stress [Eq. (29)], as $\Delta\to 0$.

The situation for $\Delta\to\infty$ is more subtle. The TSSM model fails in the long-time limit in that, by Eq. (32), the model inappropriately turns off (vanishes). An analog of this result is that the spatial ADM model also turns off whenever a spectral (sharp cut-off) filter is used, because, for such filters, $\bar{\bar{u}}=\bar{u}$ (N. A. Adams, personal communication). In general, the difficulty with sharp cut-off filters, whether spatial or temporal, is that they are noninvertible. In the long-time limit, present temporal filters necessarily act spectrally in that they preserve only the time average, in which case, in Fourier space the transfer function is a delta function at frequency zero (refer to Fig. 2). In theory then, the TADM fails also in the long-time limit because multiply filtered quantities simply replicate the long-time average. For practical applications of TLES, however, the filter width, however large, would be finite. For any finite Δ, an accurate deconvolution can be obtained provided the deconvolution order is sufficiently high. For example, Fig. 13 compares the quantities $\bar{f}$ and $\bar{v}$ for deconvolutions of differing orders. Here, f is the same time series shown in Fig. 3, $\bar{f}$ is its filtered counterpart for relatively large filter-width ratio $r=64$, and $\bar{v}$ is the filtered, deconvolved time series. Moreover, here and in the subsequent discussion, p denotes the order of the deconvolution. Note that $r=64$ results in the attenuation of nearly all high-frequency content leaving principally only a fundamental frequency. Deconvolutions of orders 1, 4, and 7 are presented. Whereas, the deconvolutions $p=1$ and $p=4$ are in poor agreement with $\bar{f}$, for $p=7$, $\bar{v}$ agrees closely with $\bar{f}$.

TABLE I. Parameter values for TLES *a posteriori* analysis cases and reference DNS case.

Case	n	Δt	r	Δ	p
DNS	256	1/256	8	1/32	NA
TLES4.1	128	1/128	4	1/32	1
TLES4.0	128	1/128	4	1/32	0
TLES2	64	1/64	2	1/32	0
TLES1	32	1/32	1	1/32	0

V. *A POSTERIORI* ANALYSIS

Section IV addressed the predictive capability of two temporal residual-stress models (TSSM and TADM) by means of *a priori* analysis. It is well known that models may perform well in *a priori* analyses yet fail in actual LES. In this section, we lend further weight to the potential of TLES by conducting *a posteriori* analyses for the forced VBE [Eq. (41)].

The governing system for TLES consists of Eq. (41), with $[\tau_R]$ replaced by $[\tau_R]_{\text{mod}}$ [Eq. (46)], coupled with filter evolution Eqs. (44) and (45). The filtered forcing function $\overline{F}$ is computed from F via an evolution equation analogous to Eq. (44). We consider only deconvolutions of orders zero and unity, $p=0$ and $p=1$, respectively. The reader is reminded that the TADM with $p=0$ is equivalent to the TSSM.

The computational methodology for the *a posteriori* analyses differs somewhat from that of the *a priori* analyses. Specifically, all equations, including the filter evolution equations, are advanced in time by RK4 methodology. Moreover, for computational efficiency, spatial derivatives are computed pseudospectrally, rather than by the Galerkin method exploited previously. For reasons to be discussed shortly, no de-aliasing procedure is implemented.

In *a posteriori* analyses, LES results are compared with results obtained by filtering a reference DNS solution *ex post facto*. Parameter values for the reference DNS and TLES cases are presented in Table I below. The reference DNS case is exactly that of Sec. IV, with the sole exception that the number of time steps per fundamental forcing period has been adjusted. For the DNS solution, both the spatial grid resolution parameter n and the number of time steps per fundamental forcing period are integer powers of two to facilitate analyses of spectra by Fourier transform methods. Spatial resolution ($n=256$) was established so that the (relative) amplitude of the highest wavenumber was approximately machine epsilon for double precision (10^{-15}). The number of time steps per fundamental period (256) was chosen to ensure eight time steps per period at the highest forced harmonic ($k_F=32$). Relative to the parameters of the reference DNS, cases TLES4, TLES2, and TLES1 represent coarsenings in both time and space by successive factors of 2. Thus, the computational effort of TLES1 is roughly 1/64th that of the reference DNS. The computational advantages, of course, are expected to grow dramatically as the number of dimensions increases. For a three-dimensional flow, the computational effort of a similarly coarsened TLES should be $(1/64)^2$ times that of a fully resolved DNS.

The DNS solution is postprocessed by filtering with filter-width ratio $r=8$, which, as will be shown, produces a substantial effect on the frequency spectrum. (Refer to Figs. 2 and 5 for the effect of filtering with $r=8$.) Comparisons of TLES4, TLES2, and TLES1 with the filtered DNS results are meaningful only if the filter width $\Delta=r\Delta t$ is the same for all cases. Accordingly, $r=4$, $r=2$, and $r=1$ for cases TLES4, TLES2, and TLES1, respectively.

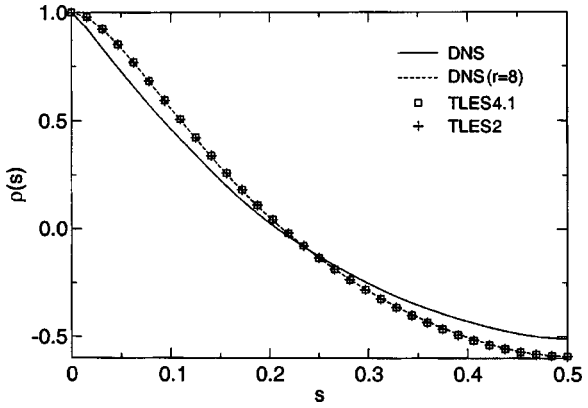

FIG. 14. Autocorrelation functions $\rho(s)$ of TLES cases compared with those of DNS and filtered DNS. For clarity, every other point shown. Note: autocorrelation is nearly periodic with nominal period unity.

Figures 14 and 15 present the autocorrelation functions and the spectra, respectively, of the DNS, the filtered DNS, and the TLES cases. Spectra are computed as cosine transforms of their respective autocovariance functions $R(s)$; that is,

$$S(\omega)=\frac{2}{\pi}\int_0^\infty R(s)\cos(\omega s)ds, \tag{48}$$

where (as before) ω is the circular frequency, and where S is used unconventionally for the frequency spectrum because of the previous use of E as expected value. The autocovariance is computed only after the solution has attained stationarity; that is for $t>200$. It was established previously that the flow is homogeneous as well as stationary. Consequently, for pur-

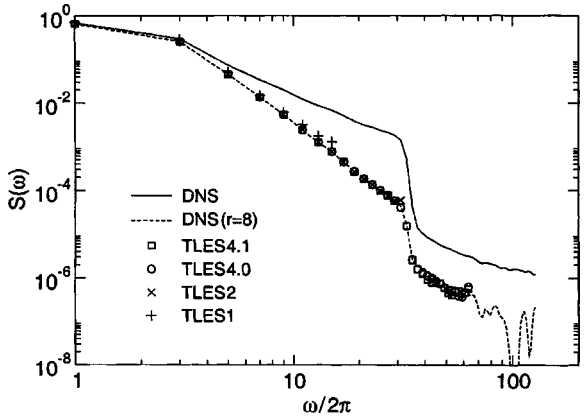

FIG. 15. Frequency spectra of TLES cases compared with that of DNS and filtered DNS. For clarity, every other point shown. Spectra terminate at frequencies $\omega/(2\pi)$ 128, 64, 32, and 16, for cases DNS (and filtered DNS), TLES4, TLES2, and TLES1, respectively.

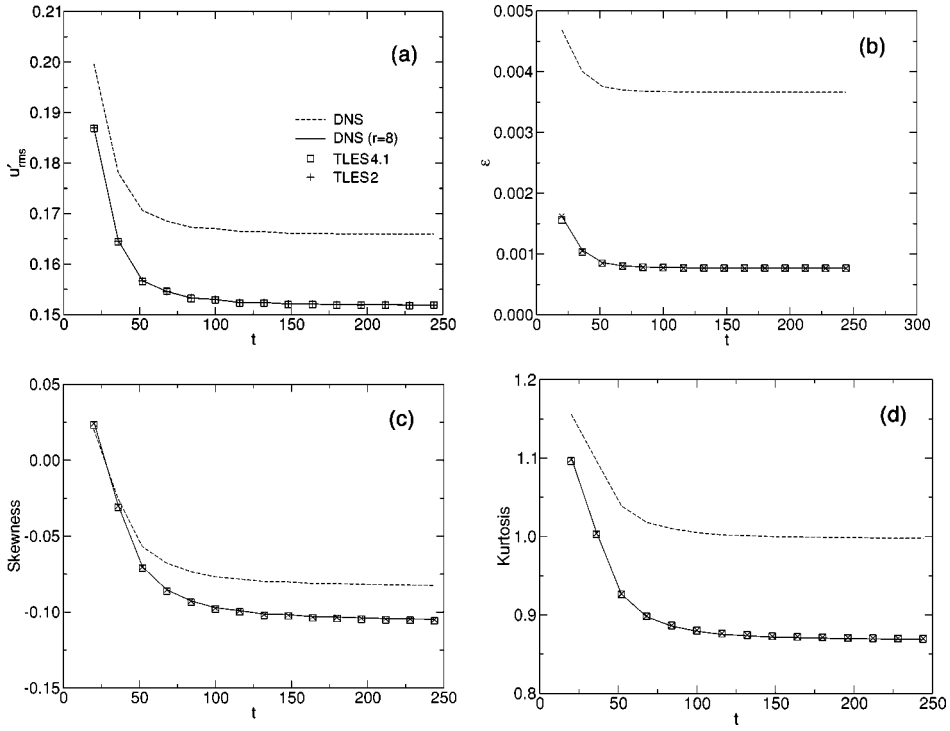

FIG. 16. Window-averaged ($\Delta=20$) turbulence quantities of selected TLES cases compared with those of filtered DNS: (a) root-mean-square velocity u'_{rms}, (b) energy dissipation rate ϵ, (c) skewness, (d) kurtosis. For reference, data extracted from Fig. 9 (DNS) are superimposed.

poses of computing the autocovariance, it suffices to record the time trace of the solution at an arbitrary value of x. If this time series is denoted simply as $u(t)$, then

$$R(s)=\langle u(t)u(t+s)\rangle_t, \tag{49}$$

where the time interval for the windowed average is $\Delta=20$.

Figure 14 compares the autocorrelation function of the TLES cases with those of the DNS and filtered DNS. The autocorrelation function $\rho(s)$ is the autocovariance normalized by the variance, and the autocorrelation of a periodic signal is itself periodic. Although the Burger's "flow" is spatially periodic and subject to periodic forcing, the output is not quite periodic because of the quadratic nonlinearity of the governing equation. Consequently, in all cases, $R(s)$ is subjected to a Parzen windowing function prior to the transform by Eq. (48).

Figure 15 compares the spectra of the TLES cases with those of the DNS and filtered DNS. The spectra of the DNS and filtered DNS differ dramatically. The TLES spectra match the filtered DNS spectrum extremely well in all cases except TLES1. Surprisingly, there is little difference in the $p=0$ and $p=1$ deconvolutions of case TLES4, with the exception of minor differences at the higher frequencies.

To avoid mixing temporal and spatial filtering and clouding the effects of (purely) temporal filtering, no de-aliasing procedures were implemented for any of the computations. The DNS computation, being well resolved, needed no de-aliasing. Cases TLES4 are also well resolved because high-frequency content is strongly attenuated by the filter. Case TLES2 is only marginally resolved. The spectrum for case TLES1, which is severely under-resolved because if fails the Nyquist criterion, agrees moderately well with that of the filtered DNS; however, it tends to overshoot at all frequencies, most likely a result of aliasing errors.

Finally, Fig. 16 compares window-averaged turbulence statistics of selected TLES cases with those of the filtered DNS. Specifically, Fig. 16, the TLES analog of Fig. 9, results from averaging the turbulence quantities over a temporal window of duration $\Delta=20$. The spectra of the filtered and unfiltered DNS solutions (Fig. 15) differ dramatically, a difference reflected in the turbulence statistics of Figs. 16 and 9, respectively. (For ease of comparison, the results of Fig. 9 are superimposed on Fig. 16.) However, Fig. 16 reveals excellent statistical agreement between cases TLES4 and TLES2 and the filtered DNS. Because of the suspected aliasing errors, case TLES1 is not presented.

Although full verification of TLES awaits simulation of three-dimensional flows at high Reynolds number, present results with forced, viscous Burger's "flow" are encouraging and suggest that TLES should be further investigated.

VI. CONCLUSIONS

The behavior of the residual stress of the temporally filtered Navier–Stokes (TFNS) equations was studied for a class of differential, causal time-domain filters parametrized by the temporal filter width Δ. The effect of filter width on the residual stress was examined for the asymptotic limits $\Delta\to 0$ and $\Delta\to\infty$ and for the case of finite filter width. It was shown analytically that, in the limit $\Delta\to 0$, the residual stress vanishes so that the Navier–Stokes equations are recovered from the temporally filtered equations. Alternately, in the limit $\Delta\to\infty$, for a statistically steady flow, the residual stress

asymptotically approaches the Reynolds stress, and the Reynolds-averaged Navier–Stokes equations are recovered from the temporally filtered equations. These asymptotic results were verified numerically through simulations of the temporally filtered forced, viscous Burger's equation. For the case of finite filter widths, two residual-stress models were considered that are temporal analogs of spatial SGS-stress models. These were a temporal scale similarity model (TSSM) and a temporal approximate deconvolution model (TADM). *A priori* and *a posteriori* analyses of these models were performed using highly accurate numerical solutions of the filtered forced, viscous Burger's equation. The models were found to approximately replicate the exact residual stress. Moreover, frequency spectra obtained from temporal LES (TLES) agreed closely with the appropriate spectrum extracted from filtered DNS.

It has been shown analytically that the residual stress of the TFNS equations is strongly dependent upon the temporal filter width. This fact, coupled with computational results from simulating the forced, viscous Burger's equation over a wide range of temporal filter widths, suggests that full simulations of the TFNS equations should behave like DNS for small temporal filter widths and like RANS for very large ones. For finite filter widths the formulation describes a temporally filtered LES or TLES. These results have provided a bridging mechanism between solutions obtained directly from the Navier–Stokes equations and those obtained from the Reynolds-averaged Navier–Stokes equations. Such ideas are being pursued further and will be the subject of a subsequent paper.

ACKNOWLEDGMENTS

C.D.P. and W.D.T. acknowledge the support of NASA Langley Research Center (LaRC) through Grant Nos. NAG-1-02033 and NAG-1-02027, respectively. C.E.G. acknowledges the support of NASA LaRC through Grant No. NAG-1-02005 and the National Science Foundation through Grant No. NSF OCE-0136403. Insights regarding the ADM method from N. A. Adams were greatly appreciated by C.D.P.

[1] U. Frisch, *Turbulence* (Cambridge University Press, Cambridge, 1995).
[2] M. Germano, U. Piomelli, P. Moin, and W. H. Cabot, "A dynamic subgrid-scale eddy viscosity model," Phys. Fluids A **3**, 1760 (1991).
[3] J. A. Domaradzki and E. M. Saiki, "A subgrid-scale model based on the estimation of unresolved scales of turbulence," Phys. Fluids **9**, 2148 (1997).
[4] S. Stolz and N. A. Adams, "An approximate deconvolution procedure for large-eddy simulation," Phys. Fluids **11**, 1699 (1999).
[5] P. Moin and J. Jimenez, "Large-eddy simulation of complex turbulent flows," AIAA Pap. No. 93-3099 (1993).
[6] M. Germano, "From RANS to DNS: Toward a bridging model," *Direct and Large-Eddy Simulation-III*, edited by P. R. Voke, N. D. Sandham, and L. Kleiser (Kluwer, Dordrecht, 1999), p. 225.
[7] M. Germano, "LES overview," in *DNS/LES Progress and Challenges*, edited by C. Liu, L. Sakell, and T. Beutner (Greyden, Columbus, OH, 2001), p. 1.
[8] R. D. Strum and D. E. Kirk, *First Principles of Discrete Systems and Digital Signal Processing* (Addison–Wesley, New York, 1988).
[9] C. D. Pruett, "On Eulerian time-domain filtering for spatial large-eddy simulation," AIAA J. **38**, 1634 (2000).
[10] G. A. Blaisdell, "Computation of discrete filters and differential operators for large-eddy simulation," *Advances in DNS/LES*, edited by C. Liu and Z. Liu (Greyden, Columbus, OH, 1997), p. 333.
[11] O. V. Vasilyev, T. S. Lund, and P. Moin, "A general class of commutative filters for LES in complex geometries," J. Comput. Phys. **141**, 82 (1998).
[12] C. D. Pruett, N. A. Adams, and J. S. Sochacki, "On Taylor-series expansions of residual stress," Phys. Fluids **13**, 2578 (2001).
[13] C. D. Pruett, "Toward the de-mystification of LES," *DNS/LES Progress and Challenges*, edited by C. Liu, L. Sakell, and T. Beutner (Greyden, Columbus, OH, 2001), p. 231.
[14] G. D. Stefano and O. V. Vasilyev, "A study of the effect of smooth filtering in LES," in Ref. 13, p. 247.
[15] C. G. Speziale, "Subgrid scale stress models for large-eddy simulation of rotating turbulent flows," Geophys. Astrophys. Fluid Dyn. **33**, 199 (1985).
[16] C. G. Speziale, "Invariance of turbulent closure models," Phys. Fluids **22**, 1033 (1979).
[17] C. G. Speziale, "Galilean invariance of subgrid-scale stress models in the large-eddy simulation of turbulence," J. Fluid Mech. **156**, 55 (1985).
[18] J. Bardina, J. H. Ferziger, and W. C. Reynolds, "Improved subgrid-scale models for large eddy simulation," AIAA Pap. No. 80-1357 (1980).
[19] V. Eswaran and S. B. Pope, "An examination of forcing in direct numerical simulations of turbulence," Comput. Fluids **16**, 257 (1988).
[20] B. Vreman, B. Geurts, and H. Huerten, "Realizability conditions for the turbulent stress tensor in large-eddy simulation," J. Fluid Mech. **278**, 351 (1994).
[21] S. Liu, C. Meneveau, and J. Katz, "On the properties of similarity subgrid-scale models as deduced from measurements in a turbulent jet," J. Fluid Mech. **275**, 83 (1994).
[22] C. D. Pruett and N. A. Adams, "*A priori* analyses of three subgrid-scale models for one-parameter families of filters," Phys. Fluids **12**, 1133 (2000).